X-ray Emission Spectroscopy Evidences a Central Carbon in the Nitrogenase Iron-Molybdenum Cofactor

Kyle M. Lancaster, *et al.*

Science **334**, 974 (2011);
DOI: 10.1126/science.1206445

30. A. K. Chippindale, J. R. Gibson, W. R. Rice, *Proc. Natl. Acad. Sci. U.S.A.* **98**, 1671 (2001).
31. See supporting material on *Science* Online.
32. R. M. Calisi, G. E. Bentley, *Horm. Behav.* **56**, 1 (2009).
33. D. S. Falconer, T. F. C. MacKay, *Introduction to Quantitative Genetics* (Pearson Prentice Hall, London, ed. 4, 1996).

Acknowledgments: Supported by Academy of Finland grants 115961, 119200, and 218107 (E.K.), 132190 (T.M.), and 103508 and 108566 (S.C.M.); the Vanamo Biological Society and Ehrnrooth Foundation (M.M.); the Australian Research Council and Australian National University (H.K. and J.L.); the Finnish Cultural Foundation and Emil Aaltonen Foundation (J.L.); and the Centre of Excellence in Evolutionary Research, University of Jyväskylä. We thank the staff of the Experimental Animal Unit and Konnevesi Research Station, University of Jyväskylä; R. Närä and H. Pietiläinen for logistical support; T. Laaksonen, V. Lummaa, and three anonymous reviewers for comments; and C. Soulsbury for statistical advice. The authors declare no conflicts of interest. All co-authors designed this study; M.M., E.K., T.M. and H.M. collected and analyzed the empirical data; J.L. analyzed theoretical results with input from all authors; and M.M. led the preparation of the manuscript with input from all co-authors. Authors after the first author are listed in alphabetical order. Data have been deposited in the Dryad Repository (doi:10.5061/dryad.6m0f6870).

Supporting Online Material
www.sciencemag.org/cgi/content/full/334/6058/972/DC1
Materials and Methods
Figs. S1 to S3
Table S1
References (*34*–*41*)

20 May 2011; accepted 29 September 2011
10.1126/science.1208708

X-ray Emission Spectroscopy Evidences a Central Carbon in the Nitrogenase Iron-Molybdenum Cofactor

Kyle M. Lancaster,[1] Michael Roemelt,[2] Patrick Ettenhuber,[2] Yilin Hu,[3] Markus W. Ribbe,[3]* Frank Neese,[2,4]* Uwe Bergmann,[5]* Serena DeBeer[1,4]*

Nitrogenase is a complex enzyme that catalyzes the reduction of dinitrogen to ammonia. Despite insight from structural and biochemical studies, its structure and mechanism await full characterization. An iron-molybdenum cofactor (FeMoco) is thought to be the site of dinitrogen reduction, but the identity of a central atom in this cofactor remains unknown. Fe Kβ x-ray emission spectroscopy (XES) of intact nitrogenase MoFe protein, isolated FeMoco, and the FeMoco-deficient Δ*nifB* protein indicates that among the candidate atoms oxygen, nitrogen, and carbon, it is carbon that best fits the XES data. The experimental XES is supported by computational efforts, which show that oxidation and spin states do not affect the assignment of the central atom to C^{4-}. Identification of the central atom will drive further studies on its role in catalysis.

Nitrogenase (N_2ase), found in symbiotic and free-living diazotrophs, catalyzes the reduction of dinitrogen (N_2) to ammonia (NH_3) using eight electrons, eight protons, and 16 MgATPs (ATP, adenosine triphosphate) (*1*). Industrially, the same reaction is performed by the Haber-Bosch process that produces more than 100 million tons of NH_3 each year, thereby accounting for ~1.4% of global energy consumption. Understanding how nature activates the strongest homodinuclear bond in chemistry, the triple bond of N_2, is the key for the future design of molecular catalysts.

The high-resolution crystal structure of N_2ase determined by Einsle *et al*. (*2*) showed that the active site of the molybdenum-iron (MoFe) protein component of N_2ase binds a complex cluster consisting of seven iron ions, one molybdenum ion, and nine sulfides (Fig. 1A); this cluster is referred to as the iron-molybdenum cofactor (FeMoco) and is thought to be the site of dinitrogen activation. For each FeMoco (of which there are two in the $\alpha_2\beta_2$ tetrameric MoFe protein) there is an additional cluster that consists of eight irons and seven sulfides (Fig. 1B); this cluster is referred to as the P cluster. The P clusters serve as electron-transfer sites. Several reaction intermediates in nitrogenase catalysis have recently been observed (*3*, *4*). However, despite the progress in the experimental and theoretical analysis of the FeMoco (*4*–*7*), neither the reaction that occurs at the FeMoco nor the structure of FeMoco has been fully clarified. In 2002, Einsle *et al*. identified a light atom in the center of FeMoco that could be attributed to a single, fully ionized C, N, or O atom (*2*). No consensus has since emerged concerning the nature of this key atom. Study of FeMoco by electron paramagnetic resonance and related techniques is complicated by complex spin-couplings between the open-shell ions, which are not fully understood. Mössbauer spectroscopy suffers from spectral crowding, and neither nuclear resonance vibrational spectroscopy nor extended x-ray absorption fine structure are sufficiently conclusive (*8*).

Herein, we report iron Kβ valence-to-core (V2C) x-ray emission spectroscopy (XES) of N_2ase and demonstrate that these data provide a signature for the presence and identity of the central atom. Kα and Kβ XES monitor the emission of photons after ionization of a metal 1s electron. The $K\beta_{1,3}$ emission line (~7040 to 7070 eV) corresponds to an electric dipole allowed 3p → 1s transition. To higher emission energies,

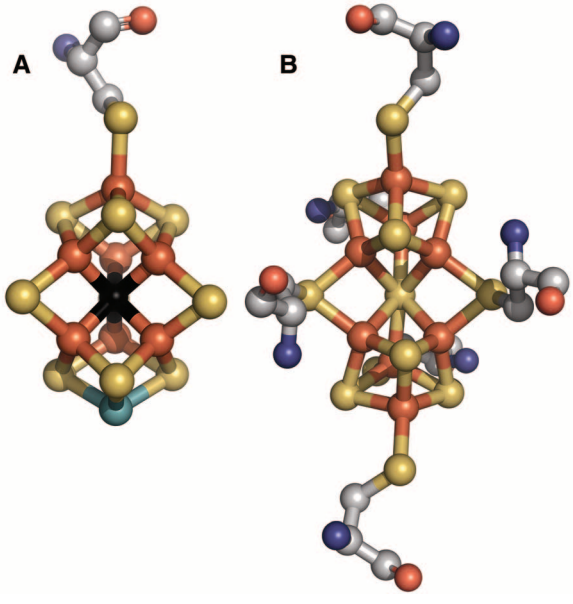

Fig. 1. The FeMoco (**A**) and P cluster (**B**) of nitrogenase (adapted from the Protein Data Bank: identification number 1MIN). Orange, Fe; yellow, S; light blue, Mo; black, C^{4-}, N^{3-}, or O^{2-}; dark blue, nitrogen; gray, carbon. For clarity, the homocitrate and histidine ligands to the Mo have been omitted.

[1]Department of Chemistry and Chemical Biology, Cornell University, Ithaca, NY 14853, USA. [2]Institut für Physikalische und Theoretische Chemie, Universität Bonn, D-53115 Bonn, Germany. [3]Department of Molecular Biology and Biochemistry, University of California, Irvine, CA 92697, USA. [4]Max-Planck-Institut für Bioanorganische Chemie, Stiftstrasse 34-36, D-45470 Mülheim an der Ruhr, Germany. [5]Linac Coherent Light Source, SLAC National Accelerator Laboratory, Menlo Park, CA 94025, USA.

*To whom correspondence should be addressed: mribbe@uci.edu (M.W.R.); frank.neese@mpi-mail.mpg.de (F.N.); bergmann@slac.stanford.edu (U.B.); serena.debeer@mpi-mail.mpg.de (S.D.)

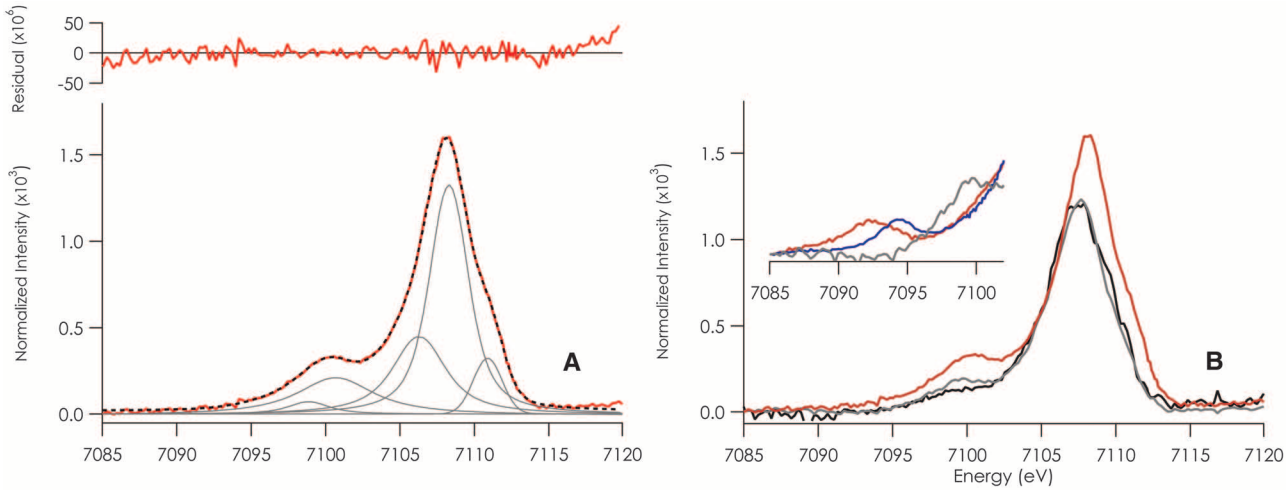

Fig. 2. (**A**) Normalized V2C XES spectra of isolated FeMoco (red) and a representative fit to the data (black dashed line). (**B**) Comparison of the normalized V2C XES data for FeMoco (red), the MoFe protein (gray), and the Δ*nifB* MoFe protein (black). (Inset) V2C satellite region for Fe_2O_3 (red), Fe_3N (blue), and MoFe protein (gray).

Table 1. V2C XES fit parameters. n/a, not applicable.

	Δ*nifB* MoFe protein		FeMoco		MoFe protein	
	E (eV)	Integrated intensity	E (eV)	Integrated intensity	E (eV)	Integrated intensity
Kβ″ peak 1	7098.8	0.30	7098.8	0.18	7098.8	0.30
Kβ″ peak 2	n/a	n/a	7100.2	1.60	7100.5	0.58
Total Kβ″ integrated intensity	n/a	0.30	n/a	1.78	n/a	0.88
Total V2C integrated intensity		7.73		10.45		7.61

valence-electron transitions into the metal 1s core hole are observed (referred to as the $K\beta_{2,5}$/Kβ″ or V2C region). These transitions have previously been assigned as ligand *n*p → metal 1s ($K\beta_{2,5}$, ~7102 to 7112 eV) and ligand *n*s → metal 1s (Kβ″ or "satellite," ~7090 to 7102 eV) transitions (*9*). V2C XES studies of Cr and Mn complexes have shown that the Kβ″ features provide a signature for the identity of the directly coordinating ligands, because energies of the observed features depend primarily on the ligand 2s ionization energies (*10*, *11*). We recently developed an experimental and theoretical protocol for the analysis of V2C XES spectra and applied it to mono- (*12*–*14*) and multinuclear (*15*) iron complexes. Of particular relevance is a study of a six-iron cluster with a central μ_6-C^{4-} (*15*). These data show a feature at 7099 eV that is attributed to a transition originating from the μ_6-C^{4-} 2s orbital. Computationally, this feature is predicted to shift to 7094 eV for a μ_6-N^{3-} and 7088 eV for a μ_6-O^{2-}. These trends closely parallel previous observations for infinite lattice complexes and mononuclear molecular complexes, thus highlighting the general applicability of this method (*11*, *12*, *16*).

Figure 2A presents the normalized V2C XES data of the isolated FeMoco of N_2ase, together with a representative fit to the data. Based on previous studies, the features observed with maxima at ~7108 and ~7100 eV are assigned to ligand *n*p and *n*s contributions, respectively (*12*). To assess the contribution of the sulfur ligands relative to the interstitial atom X, data were also obtained for the Δ*nifB* MoFe protein (Fig. 2B). This mutant contains only the two P clusters (*17*, *18*). Based on their structural similarity, it can be assumed that the P cluster and the FeMoco have similar sulfur contributions to their XES spectra; this assumption is also supported computationally (see below). Data were obtained for the intact MoFe protein (containing both clusters) (Fig. 2B). The MoFe protein spectra map well onto an average of the spectra of the P cluster (represented by the Δ*nifB* MoFe protein) and the isolated FeMoco (fig. S1).

Comparison between the data of the isolated FeMoco and that of the P clusters in the Δ*nifB* MoFe protein allowed us to assess the relative contributions of these clusters to the spectra. The V2C XES data of the P clusters showed only a weak satellite at 7098.8 with 0.30 ± 0.03 units of integrated intensity. In contrast, isolated FeMoco exhibited a well-resolved satellite feature to higher energy (7100.2 eV) with an approximately sixfold increase in the integrated intensity of the satellite feature (1.78 ± 0.18 units). To better understand the origin of these satellite features, we also compared the data for Δ*nifB* MoFe protein to the XES data for a $[Fe_4S_4(SPh)_4]^{2-}$ model complex (*19*). Both the P clusters and the Fe_4S_4 cubane have very similar XES spectra (figs. S2 and S3). Thus, the weak 7098.8-eV feature must be attributed to a S 3s → Fe 1s transition. Under the plausible assumption that the S 3s contributions to the P cluster and FeMoco V2C XES spectra are similar, we can model the satellite region with two features: one fixed at 7098.8 eV (corresponding to the S 3s contributions) and a second to higher energy (7100.2 eV) with increased intensity (1.6 units) (Fig. 2A and Table 1). The higher-energy feature is attributed to the presence of the interstitial light atom. Comparison of the energy of the 7100.2-eV satellite feature in FeMoco to the O 2s → Fe 1s (~7092 eV) and N 2s → 1s (~7095 eV) transitions observed in Fe_2O_3 and Fe_3N, respectively (Fig. 2B, inset), indicates that this feature arises from a ligand with 5- and 8-eV lower ionization potential than O or N, respectively. Therefore, this comparison argues against either N or O 2s contributions and strongly supports a C 2s → Fe 1s assignment.

Fe V2C XES spectra can be predicted surprisingly well within a simple scheme based on density functional theory (*12*). To complement the experimental data, we performed detailed calculations on the FeMoco, the P cluster, and the $[Fe_4S_4(SPh)_4]^{2-}$ model complex. The FeMoco was modeled by a structure containing 152 atoms obtained from the high-resolution crystal structure of Einsle *et al.* (*2*), which incorporates the key structural and electronic features of the system. The oxidation state of this iron-sulfur cluster in the resting state of the enzyme has not been determined unambiguously. Thus, we performed calculations for the two oxidation states that have been shown to be most likely (*20*–*22*). Although these two states differ by two units of charge, the differences in the calculated V2C XES transition energies and intensities are much smaller than the experimental resolution (fig. S6). The broken symmetry approach was used to approximate the

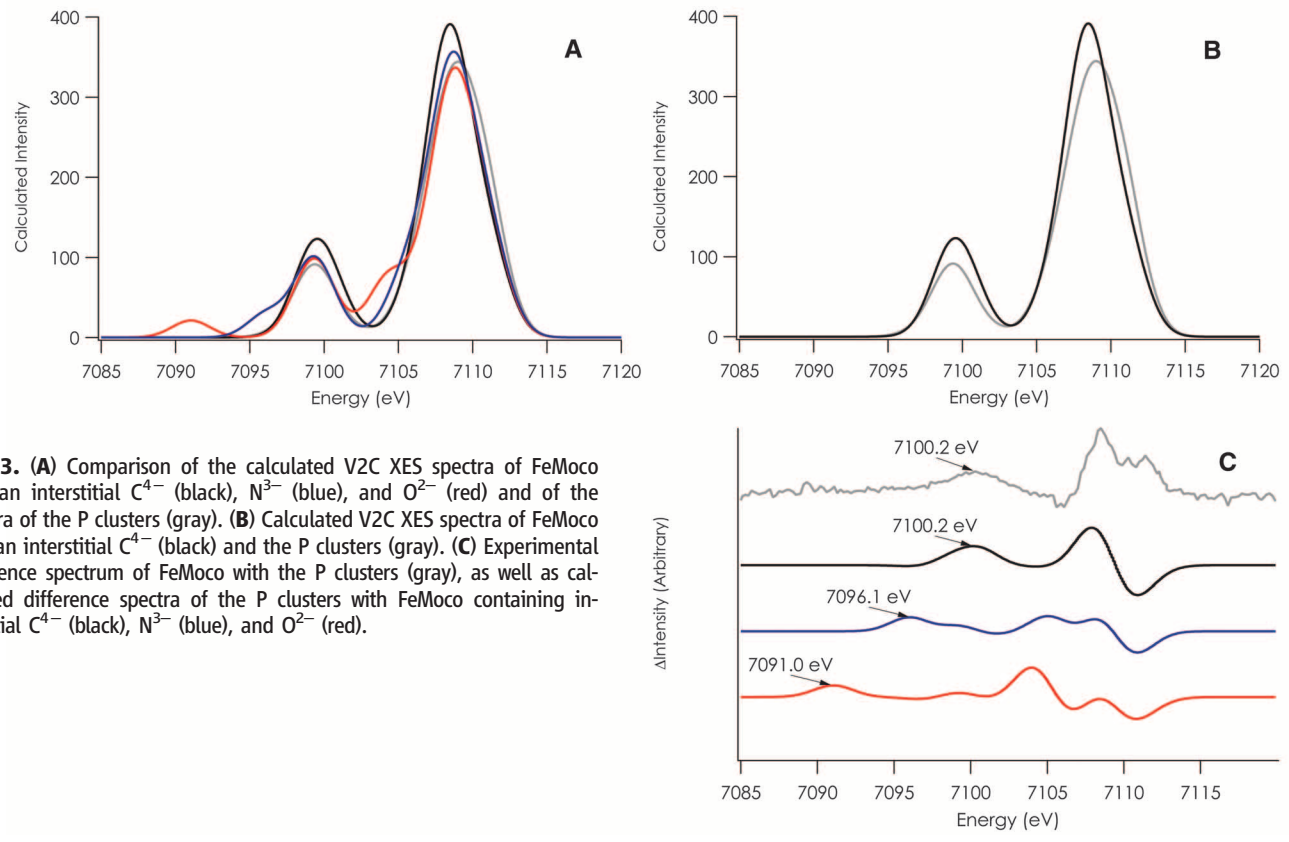

Fig. 3. (**A**) Comparison of the calculated V2C XES spectra of FeMoco with an interstitial C^{4-} (black), N^{3-} (blue), and O^{2-} (red) and of the spectra of the P clusters (gray). (**B**) Calculated V2C XES spectra of FeMoco with an interstitial C^{4-} (black) and the P clusters (gray). (**C**) Experimental difference spectrum of FeMoco with the P clusters (gray), as well as calculated difference spectra of the P clusters with FeMoco containing interstitial C^{4-} (black), N^{3-} (blue), and O^{2-} (red).

effects of magnetic coupling of the various spin centers in the FeMoco calculations (*23*). However, calculations reveal that the ligand-to-metal crossover region of the predicted V2C XES spectra is largely unaffected by magnetic coupling (fig. S7). This finding is understandable considering the large linewidth of the experimental spectra and the rather subtle differences in orbital energies arising from different magnetic coupling schemes. More importantly, the predicted V2C spectra were highly sensitive to the identity of the interstitial ion. Figure 3A presents the calculated spectra of the FeMoco, assuming interstitial O^{2-}, N^{3-}, and C^{4-} ions together with the calculated spectrum for the P cluster. As expected, all four spectra exhibit a relatively strong feature at ~7099.3 eV, corresponding to transitions from S 3s orbitals to the Fe 1s orbitals. The only exception is FeMoco with a central C^{4-} (Fig. 3B), where the maximum is slightly shifted to higher energies due to contributions from C^{4-}-related transitions in the same region. Hence, our presented data, along with analogous calculations on $[Fe_4S_4(SPh)_4]^{2-}$ (fig. S8 and S9), support the aforementioned assumption that the S peak in the V2C region appears at the same position of the spectrum for all measured species.

Subtraction of the calculated P-cluster spectrum from the calculated spectrum of the three FeMoco species yields the contributions from the respective interstitial ions (Fig. 3C). Analysis of the difference spectra reveals that the interstitial ions give rise to two features in the V2C spectrum associated with transitions from the ligand 2s and 2p orbitals, respectively. These features occur at 7096.1 and 7105.1 eV for N^{3-} and at 7091.0 and 7104.0 eV for O^{2-}. When a C^{4-} ion is placed in the center of the FeMoco, the two features are observed at 7100.2 and 7107.9 eV (Fig. 3B). For N^{3-} and C^{4-}, the higher-energy feature is not distinguishable from the large peak at ~7107 eV that is dominated by transitions originating from the S 3p orbitals.

Taken together, the experimental and theoretical results support assignment of the interstitial species as a C^{4-}. The calculated position of the C^{4-} 2s → Fe 1s peak matches the experimentally determined position at 7100.2 eV. Both N^{3-} and O^{2-} are unlikely, as their respective calculated spectra show strong features at 7096.1 eV (N^{3-} 2s) and 7091.0 eV (O^{2-} 2s). In addition, the measured spectra do not exhibit any features at lower energies than the S 3s peak, whereas such features have been observed experimentally in other N^{3-} and O^{2-} systems (as shown in the inset of Fig. 2B). The assignment is further supported by our previous studies that have shown that features with a calculated intensity of more than 10 to 15 units of intensity are experimentally observable (*12*). These studies also showed that the integrated intensities of experimental and calculated V2C agree strongly, with a 19% error for crystallographic structures. Even considering this error, the calculated low-energy features related to the N^{3-} (31 units of intensity) and O^{2-} (26 units of intensity) ions considerably exceed this threshold. In addition, several other studies on O^{2-} and N^{3-} have shown features at the corresponding energy offsets (*9*–*12*). This finding raises interesting questions about both the role of the central atom and the possible pathways for biosynthesis of such an organometallic cluster.

References and Notes

1. Y. L. Hu, M. W. Ribbe, *Acc. Chem. Res.* **43**, 475 (2010).
2. O. Einsle *et al.*, *Science* **297**, 1696 (2002).
3. B. M. Barney *et al.*, *Biochemistry* **48**, 9094 (2009).
4. B. M. Hoffman, D. R. Dean, L. C. Seefeldt, *Acc. Chem. Res.* **42**, 609 (2009).
5. D. Lukoyanov *et al.*, *Inorg. Chem.* **46**, 11437 (2007).
6. F. Neese, *Angew. Chem. Int. Ed.* **45**, 196 (2005).
7. T. V. Harris, R. K. Szilagyi, *Inorg. Chem.* **50**, 4811 (2011).
8. Y. M. Xiao *et al.*, *J. Am. Chem. Soc.* **128**, 7608 (2006).
9. P. Glatzel, U. Bergmann, *Coord. Chem. Rev.* **249**, 65 (2005).
10. G. Smolentsev *et al.*, *J. Am. Chem. Soc.* **131**, 13161 (2009).
11. S. G. Eeckhout *et al.*, *J. Anal. At. Spectrom.* **24**, 215 (2009).
12. N. Lee, T. Petrenko, U. Bergmann, F. Neese, S. DeBeer, *J. Am. Chem. Soc.* **132**, 9715 (2010).
13. C. J. Pollock, S. DeBeer, *J. Am. Chem. Soc.* **133**, 5594 (2011).
14. K. M. Lancaster, K. D. Finkelstein, S. DeBeer, *Inorg. Chem.* **50**, 6767 (2011).
15. M. U. Delgado-Jaime *et al.*, *Inorg. Chem.* 10.1021/ic201173j (2011).
16. U. Bergmann, C. R. Horne, T. J. Collins, J. M. Workman, S. P. Cramer, *Chem. Phys. Lett.* **302**, 119 (1999).
17. B. Schmid *et al.*, *Science* **296**, 352 (2002).
18. R. M. Allen, R. Chatterjee, P. W. Ludden, V. K. Shah, *J. Biol. Chem.* **270**, 26890 (1995).
19. B. A. Averill, T. Herskovitz, R. H. Holm, J. A. Ibers, *J. Am. Chem. Soc.* **95**, 3523 (1973).
20. H. I. Lee, B. J. Hales, B. M. Hoffman, *J. Am. Chem. Soc.* **119**, 11395 (1997).

21. A. E. True, M. J. Nelson, R. A. Venters, W. H. Ormejohnson, B. M. Hoffman, *J. Am. Chem. Soc.* **110**, 1935 (1988).
22. S. J. Yoo, H. C. Angove, V. Papaefthymiou, B. K. Burgess, E. Munck, *J. Am. Chem. Soc.* **122**, 4926 (2000).
23. L. Noodleman, *J. Chem. Phys.* **74**, 5737 (1981).

Acknowledgments: S.D. thanks Cornell Univ. for financial support and the Alfred P. Sloan Foundation for a fellowship; F.N. acknowledges financial support from the Univ. of Bonn, the Max Planck Society, and the SFB 813; M.W.R. thanks the NIH for funding (grant R01-GM 67626). Portions of this research were carried out at the Stanford Synchrotron Radiation Lightsource (SSRL), a U.S. Department of Energy (DOE), Basic Energy Sciences user facility. The SSRL Structural Molecular Biology program is supported by DOE, Biological and Environmental Research, and NIH, National Center for Research Resources, Biomedical Technology Program.

Supporting Online Material
www.sciencemag.org/cgi/content/full/334/6058/974/DC1
SOM Text
Figs. S1 to S11
Tables S1 and S2
References (*24*–*35*)

1 April 2011; accepted 8 September 2011
10.1126/science.1206445

Structural Basis of Silencing: Sir3 BAH Domain in Complex with a Nucleosome at 3.0 Å Resolution

Karim-Jean Armache,[1,2] Joseph D. Garlick,[1,2] Daniele Canzio,[3,4] Geeta J. Narlikar,[3] Robert E. Kingston[1,2]*

Gene silencing is essential for regulating cell fate in eukaryotes. Altered chromatin architectures contribute to maintaining the silenced state in a variety of species. The silent information regulator (Sir) proteins regulate mating type in *Saccharomyces cerevisiae*. One of these proteins, Sir3, interacts directly with the nucleosome to help generate silenced domains. We determined the crystal structure of a complex of the yeast Sir3 BAH (bromo-associated homology) domain and the nucleosome core particle at 3.0 angstrom resolution. We see multiple molecular interactions between the protein surfaces of the nucleosome and the BAH domain that explain numerous genetic mutations. These interactions are accompanied by structural rearrangements in both the nucleosome and the BAH domain. The structure explains how covalent modifications on H4K16 and H3K79 regulate formation of a silencing complex that contains the nucleosome as a central component.

Eukaryotic cells normally carry the complete set of genes needed to specify every cell type. Establishment of a specific cell fate requires the silencing of genes whose expression would disrupt that fate. Several diverse families of protein complexes maintain silencing; however, the mechanisms involved are similar in *Saccharomyces cerevisiae* and in multicellular eukaryotes (*1*). Regulation of mating type loci in *S. cerevisiae* serves as a paradigm for silencing. Yeast growing as haploids can adopt two mating types, a and α. The genes that are expressed at the *MAT* loci determine cell fate, whereas genes specifying the opposite fate can be found at the silent *HMLα* or *HMRa* loci (*1*, *2*). The silent information regulator (Sir) proteins are essential for silencing of *HMLα* and *HMRa*, as well as telomeres and the ribosomal DNA (rDNA) loci (*1*, *2*).

The Sir proteins create domains of silenced chromatin. A long-standing hypothesis is that these proteins form specific repressive architectures that involve the basic unit of chromatin, the nucleosome. In support of this hypothesis, the SIR complex or Sir3 alone can compact nucleosomal arrays in vitro (*3*–*5*). The involvement of nucleosomes in the mechanism of silencing was first indicated by the observation that yeast could not silence *HMLα* and *HMRa* when they contained a mutated form of histone H4 with a deletion of the N-terminal tail (*6*). Subsequently, specific point mutations that affected silencing were found in the N-terminal tails and in the globular portions of core histones (*7*–*14*), and deacetylation of histone H4 was identified as a hallmark of silenced regions (*15*). Reporter gene expression, restriction enzyme accessibility, and micrococcal nuclease susceptibility were used to show that domains of silenced chromatin created by the SIR complex are several kb in length (*16*–*21*).

Several aspects of the extensive body of work on Sir3 interactions with nucleosomes are especially relevant to the structural work described here. Silencing requires deacetylation of histone H4 lysine 16 (H4K16); we describe the atomic contacts in the Sir3 binding pocket for H4K16. We also describe contacts with H3K79, whose methylation has the potential to modulate silencing. Many of the mutations in histones that affect silencing lie in the LRS (loss of rDNA silencing) (*11*, *12*) domain of the nucleosome core, and we describe numerous contacts between that region and Sir3. Mutations that affect silencing have been found both at the N terminus and at the C-terminal part of Sir3 (*22*). Most of these mutations are clustered in the bromo-associated homology (BAH) domain that is found in the N terminus of Sir3 (*23*–*26*). Here, we used a mutation in Sir3 (D205N) that confers increased binding to nucleosomes in vitro. Expression of the BAH D205N domain fused to LexA partially restores silencing of mating type loci in a *sir3* null background. This domain is able, therefore, to combine with Sir2 and Sir4 to cause partial silencing when it is attached to an ectopic dimerization domain (*27*).

We report the crystal structure of the complex of the hypermorphic D205N Sir3 BAH domain (BAH_{Sir3}) and the nucleosome core particle (NCP) at 3.0 Å resolution. Details of complex reconstitution, crystallization, data collection, and refinement can be found in the supporting online material (*28*). The BAH domain interacts extensively with each of the four core histones and, consequently, the solvent-accessible surface area buried between BAH_{Sir3} and the nucleosome is large (1750 $Å^2$, probe radius 1.4 Å). The structure shows a pseudo-two-fold symmetry, similar to that seen with the RCC1-nucleosome complex (*29*), in that BAH_{Sir3} interacts in a similar manner with each of the two opposite faces of the nucleosome (Fig. 1). We observed 30 residues of BAH_{Sir3} making contacts predominately with the core histones rather than nucleosomal DNA, suggesting that this protein-protein interface is critical to silencing.

Interactions with the core histones are mediated through five regions on the surface of BAH_{Sir3}. These regions map well to contacts inferred from genetic screens (see Figs. 1D and 2B for a summary). The BAH domain interacts with the H4 tail, which becomes folded upon binding, and the regions of histones H3 and H4 that make up the LRS domain. In addition, BAH_{Sir3} contacts histone H2B at a position adjacent to the LRS surface and the H2A/H2B acidic patch. Of the histone residues contacted by BAH_{Sir3} only one residue (H4V21) varies between the *Xenopus laevis* histones used here and yeast histones (Fig. 4B and fig. S3). Both of the histone residues that can be covalently modified and participate in the regulation of silencing (*7*–*9*, *30*) (H3K79 and H4K16) are ordered in the structure (Fig. 1B and below).

Interactions between BAH_{Sir3} and the nucleosome are established through flexible regions, which fold upon interaction (Fig. 2 and Fig. 1C). The structures of both the BAH domain and the NCP alone were determined previously (*27*, *31*, *32*), allowing comparison to the structure of the complex described here. One striking transition that accompanies assembly of the complex is folding and ordering of the histone H4 tail through extended interactions with loops 2 and 4 of BAH_{Sir3} (Fig.

[1]Department of Molecular Biology, Massachusetts General Hospital, Boston, MA 02114, USA. [2]Department of Genetics, Harvard Medical School, Boston, MA 02115, USA. [3]Department of Biochemistry and Biophysics, University of California, San Francisco, San Francisco, CA 94158, USA. [4]Chemistry and Chemical Biology Graduate Program, University of California, San Francisco, San Francisco, CA 94158, USA.

*To whom correspondence should be addressed. E-mail: kingston@molbio.mgh.harvard.edu